INTERNATIONAL JOURNAL OF
NUMERICAL ANALYSIS AND MODELING
Volume 15, Number 4-5, Pages 729–745

MACRO STOKES ELEMENTS ON QUADRILATERALS

MICHAEL NEILAN AND DUYGU SAP

(Communicated by L. Rebholz)

Dedicated to Professor William J. Layton on the occasion of his 60^{th} birthday

Abstract. We construct a pair of conforming and inf–sup stable finite element spaces for the two–dimensional Stokes problem yielding divergence–free approximations on general convex quadrilateral partitions. The velocity and pressure spaces consist of piecewise quadratic and piecewise constant polynomials, respectively. We show that the discrete velocity and a locally post–processed pressure solution are second–order convergent.

Key words. Finite element analysis, divergence–free, quadrilateral mesh.

1. Introduction

In this paper we construct a low–order, conforming, inf–sup stable, and divergence–free yielding finite element method for the Stokes problem on quadrilateral partitions of $\Omega \subset \mathbb{R}^2$. Schemes satisfying these criteria, in particular the divergence–free one, have several desirable properties, for example, a decoupling of the velocity and pressure errors (cf. (22a)), the exact enforcement of several conservation laws [14], and improved long–time stability and accuracy of time–stepping schemes [4].

In more detail we propose a finite element pair $\boldsymbol{V}_h \times W_h$ consisting of piecewise polynomials with respect to a quadrilateral partition satisfying the inf–sup condition:

$$\sup_{\boldsymbol{v}\in \boldsymbol{V}_h\setminus\{0\}} \frac{\int_\Omega (\operatorname{div} \boldsymbol{v}) q\, dx}{\|\nabla \boldsymbol{v}\|_{L^2(\Omega)}} \geq \beta \|q\|_{L^2(\Omega)} \qquad \forall q \in W_h, \tag{1}$$

as well as the divergence–free property:

$$\int_\Omega (\operatorname{div} \boldsymbol{v}) q\, dx = 0 \quad \forall q \in W_h \quad \Longleftrightarrow \quad \operatorname{div} \boldsymbol{v} \equiv 0 \text{ in } L^2(\Omega). \tag{2}$$

We note that these two properties are antithetical to each other in the sense that (2) is equivalent to the inclusion $\operatorname{div} \boldsymbol{V}_h \subseteq W_h$, whereas (1) requires $W_h \subseteq \mathbb{P}_W(\operatorname{div} \boldsymbol{V}_h)$, where $\mathbb{P}_W$ denotes the L^2–projection onto W_h.

The construction of our finite element pairs is motivated by a smooth de Rham complex (or Stokes complex [15]) given by the sequence of mappings

$$0 \xrightarrow{\subset} H_0^2(\Omega) \xrightarrow{\mathbf{curl}} \boldsymbol{H}_0^1(\Omega) \xrightarrow{\operatorname{div}} L_0^2(\Omega) \longrightarrow 0, \tag{3}$$

where $\mathbf{curl} = (\partial/\partial x_2, -\partial/\partial x_1)^T$. If the domain is simply connected, then this complex is exact, i.e., the range of each map is the kernel of the succeeding map. The exactness property implies that the divergence operator is surjective from $\boldsymbol{H}_0^1(\Omega)$ onto $L_0^2(\Omega)$, and in addition, implies the existence of a stream function for incompressible flows. To ensure the stability of our finite element method and to construct

Received by the editors December 1, 2016 and, in revised form, April 5, 2017.
1991 *Mathematics Subject Classification.* 65N30.

divergence-free approximations, we build an exact subsequence of (3):

$$0 \xrightarrow{\subset} \Sigma_h \xrightarrow{\mathbf{curl}} \boldsymbol{V}_h \xrightarrow{\text{div}} W_h \longrightarrow 0, \tag{4}$$

where $\Sigma_h \subset H_0^2(\Omega)$, $\boldsymbol{V}_h \subset \boldsymbol{H}_0^1(\Omega)$ and $W_h \subset L_0^2(\Omega)$ are finite dimensional spaces consisting of piecewise polynomials. Note that the implied inclusion div $\boldsymbol{V}_h \subseteq W_h$ in (4) yields pointwise divergence–free approximations. In addition, if the subcomplex (4) is exact, then the mapping div : $\boldsymbol{V}_h \to W_h$ is surjective, and thus div $\boldsymbol{V}_h = W_h$. Along with a uniform bound of the right-inverse, this result implies the inf-sup condition (1). A key feature of this methodology is that the complex provides a guiding tool to develop a pair $\boldsymbol{V}_h \times W_h$ satisfying inf–sup stability and the divergence–free criterion. In particular, the H^2–conforming relative Σ_h dictates both the local and global properties of these spaces. As far as we are aware, all divergence-free yielding Stokes pairs follow this program, i.e., all finite element pairs $\boldsymbol{V}_h \times W_h$ satisfying div $\boldsymbol{V}_h = W_h$ have an H^2–conforming relative satisfying the exact sequence (4) (see, e.g., [3, 22, 15, 6, 17, 14, 20]).

A disadvantage of divergence–free yielding and conforming finite element pairs is that they tend to be high–order or require certain meshes to ensure stability and conformity. For example, on general triangular partitions, and for piecewise polynomial spaces, the minimal polynomial degree for the velocity space is four [22, 15]. For tensor product meshes, the smallest local velocity space in two dimensions is $\mathcal{Q}_{3,2} \times \mathcal{Q}_{2,3}$ [3, 6, 14, 20, 25], and the construction of these elements does not extend to general convex quadrilaterals defined by bilinear mappings. On the other hand, a *nonconforming* finite element method that imposes the divergence–free constraint pointwise on each quadrilateral element has recently been done in [26]. The method given there is low–order and is applicable to convex quadrilaterals. However, due to the nonconformity, the error estimates of this method are still coupled with a negative scaling of the viscosity.

We address some of these shortcomings by introducing a conforming finite element pair that yields divergence–free approximations, and in addition, is relatively low–order and stable on general shape–regular quadrilateral partitions. In our approach we take the H^2 finite element relative Σ_h in (4) to be the de Verbeke–Sanders macro element, a globally C^1 piecewise cubic spline [11, 10, 18, 21]. Via the subcomplex (4) we are then led to a piecewise quadratic (macro) velocity space and a piecewise constant pressure space. The global dimension of the spaces is comparable to the lowest–order Taylor–Hood pair [23], and furthermore, because the velocity error is decoupled from the pressure, the method still enjoys second–order accuracy. We also show that a locally computed post-processed pressure solution has second order accuracy. We mention that the use of macro elements on simplicial partitions has recently been done in [1, 7]. The work presented here complements and extends these results to quadrilateral meshes.

The rest of the paper is organized as follows. In Section 2 we set the notation and give some preliminary results. We define the finite element spaces and provide a unisolvent set of degrees of freedom in Section 3. In Section 4 we prove that the Stokes pair is inf–sup stable, and carry out a convergence analysis for the discrete problem. In addition we propose a local post–processed pressure solution that is second–order accurate.

2. Preliminaries

The two-dimensional Stokes problem with no-slip boundary conditions is given by:

$$-\nu\Delta \boldsymbol{u} + \nabla p = \boldsymbol{f}, \qquad \text{in } \Omega, \tag{5a}$$

$$\operatorname{div} \boldsymbol{u} = 0, \qquad \text{in } \Omega, \tag{5b}$$

$$\boldsymbol{u} = \boldsymbol{0}, \qquad \text{on } \partial\Omega, \tag{5c}$$

where $\Omega \subset \mathbb{R}^2$ is an open, bounded, polygonal domain, $\nu > 0$ is the viscosity, $\boldsymbol{f} \in \boldsymbol{L}^2(\Omega)$ is an external force applied to the fluid, and $\boldsymbol{u}$ and p are the velocity and the pressure of the fluid, respectively. For simplicity, we assume that ν is constant. The weak formulation for problem (5) reads: Find $(\boldsymbol{u}, p) \in \boldsymbol{H}_0^1(\Omega) \times L_0^2(\Omega)$ such that

$$\int_\Omega \nu \nabla \boldsymbol{u} : \nabla \boldsymbol{v}\, dx - \int_\Omega (\operatorname{div} \boldsymbol{v}) p\, dx = \int_\Omega \boldsymbol{f} \cdot \boldsymbol{v}\, dx, \qquad \forall \boldsymbol{v} \in \boldsymbol{H}_0^1(\Omega), \tag{6a}$$

$$\int_\Omega (\operatorname{div} \boldsymbol{u}) q\, dx = 0, \qquad \forall q \in L_0^2(\Omega), \tag{6b}$$

where $L_0^2(\Omega)$ denotes the space of square integrable functions with vanishing mean. Note that we denote vector–valued functions and vector-valued function spaces in boldface, e.g., $\boldsymbol{u}$ represents a vector–valued function and $\boldsymbol{H}^1(\Omega) = [H^1(\Omega)]^2$.

Let $\mathcal{T}_h$ denote a shape–regular quadrilateral mesh of Ω where each element in $\mathcal{T}_h$ is a convex quadrilateral. The sets of vertices and boundary vertices are given by $\mathcal{V}_h$ and $\mathcal{V}_b$, respectively. For a vertex $a \in \mathcal{V}_h$, we let $\mathcal{T}_a$ (resp., $\mathcal{E}_a$) denote the set of quadrilaterals (resp., edges) that have a as a vertex. We further denote by $\mathcal{E}_a^b$ the set of boundary edges in $\mathcal{E}_a$. For each $K \in \mathcal{T}_h$, we denote by $K_r := \{K_i\}_{i=1}^4$ the set of triangles obtained by drawing in the two diagonals between opposite vertices. The (interior) point of intersection of these two diagonals is denoted by c_K. We assume that the partition is labeled such that K_i and K_{i+1} have a common (interior) edge. The sets of vertices and edges of K are given by $\mathcal{V}_K$ and $\mathcal{E}_K$, respectively. We set h_K and h_e to be the diameter of K and length of $e \in \mathcal{E}_K$, respectively, $h := \max_{K \in \mathcal{T}_h} h_K$, and note that $h_K \approx h_e$ due to the shape–regularity of $\mathcal{T}_h$.

Let $\mathcal{P}_k(K)$ be the space of polynomials on K with degree not exceeding k, and let

$$\mathcal{P}_k(K_r) = \prod_{i=1}^4 \mathcal{P}_k(K_i), \quad \text{and} \quad \mathcal{P}_k(\mathcal{T}_h) = \prod_{K \in \mathcal{T}_h} \mathcal{P}_k(K)$$

be the corresponding (discontinuous) piecewise polynomial spaces.

Let $K_\pm \in \mathcal{T}_h$ be two elements in the mesh that share a common edge with $e = \partial K_+ \cap \partial K_-$. Assuming that the global labeling number of K_+ is smaller than that of K_-, we define the jump of a scalar or vector–valued function v as

$$[v]|_e := v_+ - v_-,$$

where $v_\pm = v|_{K_\pm}$. For a boundary edge $e = \partial K_+ \cap \partial\Omega$ we set

$$[v]|_e = v_+.$$

Let $\mathbb{P}_{1,K} : \boldsymbol{L}^2(K) \to \boldsymbol{\mathcal{P}}_1(K)$ denote the L^2 projection onto the space of linear polynomials, i.e.,

$$\int_K \mathbb{P}_{1,K} \boldsymbol{v} \cdot \boldsymbol{w}\, dx = \int_K \boldsymbol{v} \cdot \boldsymbol{w}\, dx \qquad \forall \boldsymbol{w} \in \boldsymbol{\mathcal{P}}_1(K).$$

We also set $\mathbb{P}_1 : \boldsymbol{L}^2(\Omega) \to \boldsymbol{\mathcal{P}}_1(\mathcal{T}_h)$ via $\mathbb{P}_1|_K = \mathbb{P}_{1,K}$ for all $K \in \mathcal{T}_h$. For $\boldsymbol{v} \in \boldsymbol{H}^s(K)$ and $\ell = \min\{2, s\}$, the L^2 projection satisfies [13]:

$$\|\boldsymbol{v} - \mathbb{P}_{1,K}\boldsymbol{v}\|_{L^2(K)} \le c h_K^{\ell} |\boldsymbol{v}|_{H^{\ell}(K)}, \qquad \ell = \min\{2, s\}. \tag{7}$$

This result also implies approximation properties of the L^2 projection with respect to the H^1 norm.

Lemma 2.1. *The local L^2 projection satisfies*

$$\|\nabla(\boldsymbol{v} - \mathbb{P}_{1,K}\boldsymbol{v})\|_{L^2(K)} \le C h_K^{s-1} |\boldsymbol{v}|_{H^s(K)}, \quad \forall \boldsymbol{v} \in \boldsymbol{H}^s(K),\ s = 1, 2. \tag{8}$$

Proof. Using the triangle inequality and inverse estimates, there holds for arbitrary $\boldsymbol{w} \in \boldsymbol{\mathcal{P}}_1(K)$,

$$\begin{aligned}
&\|\nabla(\boldsymbol{v} - \mathbb{P}_{1,K}\boldsymbol{v})\|_{L^2(K)} \\
\le&\|\nabla(\boldsymbol{v} - \boldsymbol{w})\|_{L^2(K)} + C h_K^{-1} \|\boldsymbol{w} - \mathbb{P}_{1,K}\boldsymbol{v}\|_{L^2(K)} \\
\le&\|\nabla(\boldsymbol{v} - \boldsymbol{w})\|_{L^2(K)} + C h_K^{-1} \big(\|\boldsymbol{v} - \boldsymbol{w}\|_{L^2(K)} + \|\boldsymbol{v} - \mathbb{P}_{1,K}\boldsymbol{v}\|_{L^2(K)}\big).
\end{aligned}$$

Standard approximation theory (cf. [13, 8]) and (7) then yield (8). □

3. Finite Element Spaces

To develop a divergence–free conforming pair for the Stokes problem, we first consider the local C^1 macro element constructed by de Verbeke and Sander [21, 11]:

$$\Sigma(K) = \mathcal{P}_3(K_r) \cap H^2(K) = \mathcal{P}_3(K_r) \cap C^1(K).$$

The dimension of $\Sigma(K)$ and a unisolvent set of degrees of freedom is given in the following lemma.

Lemma 3.1. *The dimension of $\Sigma(K)$ is 16, and a function $\psi \in \Sigma(K)$ is uniquely determined by the degrees of freedom (cf. Figure 1)*

$$D^{\alpha}\psi(a), \quad |\alpha| \le 1,\ a \in \mathcal{V}_K, \quad \text{and} \quad \int_e \frac{\partial \psi}{\partial \boldsymbol{n}_e}\, ds, \quad e \in \mathcal{E}_K, \tag{9}$$

where $\boldsymbol{n}_e$ denotes the outward unit normal of e.

Proof. A proof of this result is given in [21, 11] (also see [12]), but we provide one here for completeness.

Since the dimension of $\mathcal{P}_3(K)$ is 10, we see that $\dim \mathcal{P}_3(K_r) = 40$. The given data (9) represents 28 equations. Since the point c_K is a singular vertex (with respect to the partition $\{K_i\}_{i=1}^4$), the imposed C^1 continuity at this point represents 8 additional equations (see [19] for details). Finally the imposed C^1 continuity at the interior edge midpoints represent 4 more, for a total of 40 equations. Therefore it suffices to show that $\varphi \in \Sigma(K)$ vanishes on (9) only if $\varphi \equiv 0$.

Let $\mu \in \mathcal{P}_1(K_r) \cap H_0^1(K)$ be the unique continuous, piecewise linear polynomial that vanishes on ∂K and takes the value one at c_K. Then if $\varphi \in \Sigma(K)$ vanishes on (9), we have $\varphi = \mu^2 p$ for some $p \in \mathcal{P}_1(K_r) \cap H^1(K)$.

Denote by $\mu_i, p_i \in \mathcal{P}_1(K_i)$ as the restrictions of μ_i and p_i to K_i, respectively. Let $\ell_i = \partial K_i \cap \partial K_{i+1}$ be the common interior edge of triangles K_i and K_{i+1}. Then, due to the C^1 continuity of φ, we find that

$$\nabla \varphi|_{\ell_i} = \begin{cases} (2\mu p \nabla \mu_i + \mu^2 \nabla p_i)|_{\ell_i}, \\ (2\mu p \nabla \mu_{i+1} + \mu^2 \nabla p_{i+1})|_{\ell_i}, \end{cases}$$

and therefore $2p\nabla\mu_i + \mu\nabla p_i = 2p\nabla\mu_{i+1} + \mu\nabla p_{i+1}$ on ℓ_i. Note that $\mu = 0$ at the vertices of K and that $\nabla\mu_i$ is parallel to the normal direction of the edge $\partial K \cap \partial K_i$, in particular, $\nabla\mu_i \ne \nabla\mu_{i+1}$. It then follows from the identity $\big(2p\nabla(\mu_i - \mu_{i+1}) +$

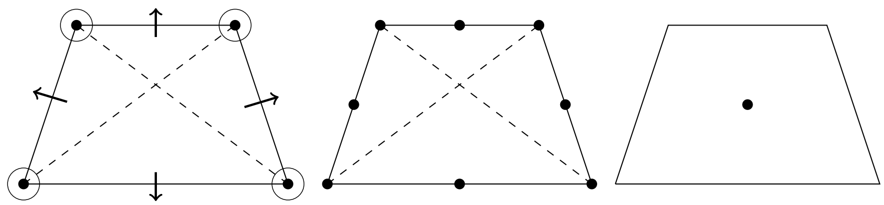

FIGURE 1. A pictorial description of the local space $\Sigma(K)$ (left), $\boldsymbol{V}(K)$ (middle), and $W(K)$ (right). Solid circles indicate function evaluations, larger circles indicate gradient evaluations, and the arrows indicate the means of the normal derivative across edges.

$\mu\nabla(p_i - p_{i+1})\big)|_{\ell_i} = 0$ that p vanishes at the vertices of K, and therefore $p = c\mu$ for some $c \in \mathbb{R}$. Thus, $\varphi = c\mu^3$. However, a simple calculation shows that $\mu^3 \notin C^1(K)$, and so we conclude that $c = 0$ and $\varphi = 0$. □

Corollary 3.2. *There holds* $\Sigma(K) \cap H_0^2(K) = \{0\}$.

Proof. If $\varphi \in \Sigma(K) \cap H_0^2(K)$, then φ vanishes on the degrees of freedom (9). By Lemma 3.1 we conclude that $\varphi \equiv 0$. □

Motivated by the smooth de Rham complex (3) and the local space $\Sigma(K)$, a natural candidate for the local Stokes pair is $(\boldsymbol{\mathcal{P}}_2(K_r) \cap \boldsymbol{H}^1(K)), \mathcal{P}_1(K_r))$. Indeed, we clearly have div : $\boldsymbol{\mathcal{P}}_2(K_r) \cap \boldsymbol{H}^1(K) \to \mathcal{P}_1(K_r)$, and **curl** : $\Sigma(K) \to \boldsymbol{\mathcal{P}}_2(K_r) \cap \boldsymbol{H}^1(K)$. Moreover, if $\boldsymbol{v} \in \boldsymbol{\mathcal{P}}_2(K_r) \cap \boldsymbol{H}^1(K)$ is divergence–free, then $\boldsymbol{v} = \mathbf{curl}\,\varphi$ for some $\varphi \in H^2(K)$. Since $\boldsymbol{v}$ is a piecewise quadratic polynomial, we conclude that φ is a piecewise cubic polynomial; thus $\varphi \in \Sigma(K)$. Therefore the kernel of the divergence operator acting on $\boldsymbol{\mathcal{P}}_2(K_r) \cap \boldsymbol{H}^1(K)$ is exactly $\mathbf{curl}\,\Sigma(K)$. However, the dimension arguments below show that $(\boldsymbol{\mathcal{P}}_2(K_r) \cap \boldsymbol{H}^1(K)), \mathcal{P}_1(K_r))$ is *not* locally inf-sup stable, and thus neither is the corresponding global pair.

Lemma 3.3. *The space* div $(\boldsymbol{\mathcal{P}}_2(K_r) \cap \boldsymbol{H}^1(K))$ *has dimension* 11. *Therefore,* div : $\boldsymbol{\mathcal{P}}_2(K_r) \cap \boldsymbol{H}^1(K) \to \mathcal{P}_1(K_r)$ *is not surjective, and thus* $(\boldsymbol{\mathcal{P}}_2(K_r) \cap \boldsymbol{H}^1(K)) \times \mathcal{P}_1(K_r)$ *does not satisfy a local inf–sup condition.*

Proof. Set $\boldsymbol{Z}_r(K) = \{\boldsymbol{v} \in \boldsymbol{\mathcal{P}}_2(K_r) \cap \boldsymbol{H}^1(K) : \operatorname{div} \boldsymbol{v} = 0\}$ to be the kernel of the divergence operator acting on $\boldsymbol{\mathcal{P}}_2(K_r) \cap \boldsymbol{H}^1(K)$. Then by the preceding discussion we have $\boldsymbol{Z}_r(K) = \mathbf{curl}\,\Sigma(K)$. Since the dimension of $\boldsymbol{\mathcal{P}}_2(K_r) \cap \boldsymbol{H}^1(K)$ is 26, we have by the rank-nullity theorem and Lemma 3.1,

$$\begin{aligned} \dim\left(\operatorname{div}\left(\boldsymbol{\mathcal{P}}_2(K_r) \cap \boldsymbol{H}^1(K)\right)\right) &= \dim(\boldsymbol{\mathcal{P}}_2(K_r) \cap \boldsymbol{H}^1(K)) - \dim \boldsymbol{Z}_r(K) \\ &= \dim\left(\boldsymbol{\mathcal{P}}_2(K_r) \cap \boldsymbol{H}^1(K)\right) - \dim\left(\mathbf{curl}(\Sigma(K))\right), \\ &= \dim\left(\boldsymbol{\mathcal{P}}_2(K_r) \cap \boldsymbol{H}^1(K)\right) - \dim \Sigma(K) + 1 = 11. \end{aligned}$$

Because $\dim \mathcal{P}_1(K_r) = 12$, we conclude that the divergence operator mapping $\boldsymbol{\mathcal{P}}_2(K_r) \cap \boldsymbol{H}^1(K)$ to $\mathcal{P}_1(K_r)$ is not surjective. Furthermore, the dimension count shows that there exists $q \in \mathcal{P}_1(K_r)$ such that $\int_K (\operatorname{div} \boldsymbol{v}) q\, dx = 0$ for all $\boldsymbol{v} \in \boldsymbol{\mathcal{P}}_2(K_r) \cap \boldsymbol{H}^1(K)$, and therefore the pair $(\boldsymbol{\mathcal{P}}_2(K_r) \cap \boldsymbol{H}^1(K)) \times \mathcal{P}_1(K_r)$ does not satisfy a local inf–sup condition. □

Remark 3.4. *By* [24, Proposition 2.1]*, the range of the divergence operator is characterized as*

$$\mathrm{div}\,(\boldsymbol{\mathcal{P}}_2(K_r)\cap \boldsymbol{H}^1(K)) = \{q\in \mathcal{P}_1(K_r) : \sum_{i=1}^4 (-1)^i q|_{K_i}(c_K) = 0\}.$$

3.1. The local velocity space. To derive a locally stable finite element based on the de Verbeke–Sanders element, we simply restrict the range of the divergence operator and consider the finite element space

$$\boldsymbol{V}(K) = \{\boldsymbol{v}\in \boldsymbol{\mathcal{P}}_2(K_r)\cap \boldsymbol{H}^1(K) : \mathrm{div}\,\boldsymbol{v}\in \mathcal{P}_0(K)\}. \tag{10}$$

A unisolvent set of degrees of freedom is given in the next lemma.

Lemma 3.5. *The dimension of* $\boldsymbol{V}(K)$ *is* 16*, and a function* $\boldsymbol{v}\in\boldsymbol{V}(K)$ *is uniquely determined by the values*

$$\boldsymbol{v}(a),\quad a\in\mathcal{V}_K,\quad \textit{and}\quad \int_e \boldsymbol{v}\,ds,\quad e\in\mathcal{E}_K. \tag{11}$$

Proof. We easily find that the kernel of the divergence operator acting on $\boldsymbol{V}(K)$ is given by $\boldsymbol{Z}_r(K) = \mathbf{curl}\,\Sigma(K)$. Therefore by the rank–nullity theorem, we have

$$\begin{aligned}\dim \boldsymbol{V}(K) &= \dim \mathbf{curl}(\Sigma(K)) + \dim \mathcal{P}_0(K)\\ &= \dim\Sigma(K) + \dim\mathcal{P}_0(K) - 1 = 16.\end{aligned}$$

Since 16 conditions are given in (11) it suffices to show that if $\boldsymbol{v}\in\boldsymbol{V}(K)$ vanishes on (11), then $\boldsymbol{v}\equiv\boldsymbol{0}$.

If $\boldsymbol{v}\in\boldsymbol{V}(K)$ vanishes on (11), then $\boldsymbol{v}\in\boldsymbol{V}(K)\cap\boldsymbol{H}_0^1(K)$ since $\boldsymbol{v}$ is piecewise quadratic. Therefore by the divergence theorem

$$\int_K \mathrm{div}\,\boldsymbol{v}\,dx = \int_{\partial K}\boldsymbol{v}\cdot\boldsymbol{n}\,ds = 0.$$

Since $\mathrm{div}\,\boldsymbol{v}$ is constant, we conclude that $\boldsymbol{v}$ is divergence–free. Thus, $\boldsymbol{v} = \mathbf{curl}\,\varphi$ for some $\varphi\in\Sigma(K)$, and since $\boldsymbol{v}\in\boldsymbol{H}_0^1(K)$, we may assume that $\varphi\in\Sigma(K)\cap H_0^2(K)$. But then Corollary 3.2 shows that $\varphi\equiv 0$, and therefore $\boldsymbol{v}\equiv\boldsymbol{0}$. ☐

4. Stability and Convergence Analysis

The local spaces and degrees of freedom lead to the following global spaces for the Stokes problem:

$$\begin{aligned}\boldsymbol{V}_h &= \{\boldsymbol{v}\in\boldsymbol{H}_0^1(\Omega) : \boldsymbol{v}|_K\in\boldsymbol{V}(K),\ \forall K\in\mathcal{T}_h\},\\ W_h &= \{q\in L_0^2(\Omega) : q|_K\in\mathcal{P}_0(K),\ \forall K\in\mathcal{T}_h\}.\end{aligned}$$

We also define the corresponding C^1 finite element space as

$$\Sigma_h := \{z\in H_0^2(\Omega) :\ z|_K\in\Sigma(K),\ \forall K\in\mathcal{T}_h\}.$$

Analogous to the continuous setting (cf. (3)), the finite element spaces form an exact sequence.

Lemma 4.1. *Suppose that the domain is simply connected. Then the sequence* (4) *is exact.*

Proof. It is clear from the definitions of the finite element spaces that if $\boldsymbol{v}\in\boldsymbol{V}_h$ is divergence–free, then $\boldsymbol{v} = \mathbf{curl}\,\varphi$ for some $\varphi\in\Sigma_h$.

Let $\mathring{\mathbb{V}}$, $\mathring{\mathbb{E}}$, and $\mathbb{K}$ denote the number of interior vertices, interior edges, and quadrilaterals in the mesh $\mathcal{T}_h$, respectively. From Lemmas 3.1 and 3.5, we find that $\dim \Sigma_h = 3\mathring{\mathbb{V}} + \mathring{\mathbb{E}}$ and $\dim \boldsymbol{V}_h = 2\mathring{\mathbb{V}} + 2\mathring{\mathbb{E}}$. Therefore, by the rank–nullity theorem,

$$\dim(\operatorname{div} \boldsymbol{V}_h) = \dim \boldsymbol{V}_h - \dim(\mathbf{curl}\,\Sigma_h) = \dim \boldsymbol{V}_h - \dim \Sigma_h = \mathring{\mathbb{E}} - \mathring{\mathbb{V}}.$$

Using the Euler identity $\mathring{\mathbb{E}} = \mathbb{K} + \mathring{\mathbb{V}} - 1$ on simply connected domains [18, Lemma 4.41], and since clearly $\dim W_h = \mathbb{K} - 1$, we get $\dim(\operatorname{div} \boldsymbol{V}_h) = \dim W_h$. Since $\operatorname{div} \boldsymbol{V}_h \subseteq W_h$, we conclude that $\operatorname{div} \boldsymbol{V}_h = W_h$. Therefore the sequence (4) is exact. □

The proceeding lemma shows that the divergence operator, acting on $\boldsymbol{V}_h$, is surjective onto W_h provided that Ω is simply connected. The next result shows that this property holds on general Lipschitz domains, and in addition, gives a uniform bound on the right–inverse.

Lemma 4.2. *Denote by $\mathbb{P}_W : L^2_0(\Omega) \to W_h$ the L^2–projection onto W_h. Then there exists a (Fortin) operator $\boldsymbol{\Pi}_{\boldsymbol{V}} : \boldsymbol{H}^1_0(\Omega) \to \boldsymbol{V}_h$ such that $\operatorname{div} \boldsymbol{\Pi}_{\boldsymbol{V}} \boldsymbol{v} = \mathbb{P}_W \operatorname{div} \boldsymbol{v}$ and $\|\nabla \boldsymbol{\Pi}_{\boldsymbol{V}} \boldsymbol{v}\|_{L^2(\Omega)} \le C\|\nabla \boldsymbol{v}\|_{L^2(\Omega)}$ for all $\boldsymbol{v} \in \boldsymbol{H}^1_0(\Omega)$. Consequently, $\boldsymbol{V}_h \times W_h$ is an inf–sup stable finite element pair.*

Proof. Define $\boldsymbol{\Pi}_{\boldsymbol{V}} : \boldsymbol{H}^1_0(\Omega) \to \boldsymbol{V}_h$ such that it satisfies

$$\int_e \boldsymbol{\Pi}_{\boldsymbol{V}} \boldsymbol{v}\, ds = \int_e \boldsymbol{v}\, ds, \qquad \forall e \in \mathcal{E}_K, \forall K \in \mathcal{T}_h, \tag{12a}$$

$$\boldsymbol{\Pi}_{\boldsymbol{V}} \boldsymbol{v}(a) = \frac{1}{|\mathcal{T}_a|} \sum_{K' \in \mathcal{T}_a} \mathbb{P}_{1,K'} \boldsymbol{v}(a), \quad \forall a \in \mathcal{V}_K \setminus \mathcal{V}_b, \forall K \in \mathcal{T}_h, \tag{12b}$$

$$\boldsymbol{\Pi}_{\boldsymbol{V}} \boldsymbol{v}(a) = 0, \qquad \forall a \in \mathcal{V}_b, \tag{12c}$$

where $|\mathcal{T}_a|$ is the cardinality of the set $\mathcal{T}_a$.

By the divergence theorem and (12a),

$$\int_K \operatorname{div}(\boldsymbol{\Pi}_{\boldsymbol{V}} \boldsymbol{v})\, dx = \int_{\partial K} (\boldsymbol{\Pi}_{\boldsymbol{V}} \boldsymbol{v}) \cdot \boldsymbol{n}\, ds = \int_{\partial K} (\boldsymbol{v} \cdot \boldsymbol{n}) ds = \int_K \operatorname{div} \boldsymbol{v}\, dx \qquad \forall K \in \mathcal{T}_h. \tag{13}$$

Thus, $\operatorname{div} \boldsymbol{\Pi}_{\boldsymbol{V}} \boldsymbol{v} = \mathbb{P}_W(\operatorname{div} \boldsymbol{v})$.

Next we write, using Lemma 2.1,

$$\begin{aligned} \|\nabla \boldsymbol{\Pi}_{\boldsymbol{V}} \boldsymbol{v}\|^2_{L^2(\Omega)} &\le 2 \sum_{K \in \mathcal{T}_h} (\|\nabla(\boldsymbol{\Pi}_{\boldsymbol{V}} \boldsymbol{v} - \mathbb{P}_{1,K} \boldsymbol{v})\|^2_{L^2(K)} + \|\nabla \mathbb{P}_{1,K} \boldsymbol{v}\|^2_{L^2(K)}) \\ &\le C\|\nabla \boldsymbol{v}\|^2_{L^2(\Omega)} + 2 \sum_{K \in \mathcal{T}_h} \|\nabla(\boldsymbol{\Pi}_{\boldsymbol{V}} \boldsymbol{v} - \mathbb{P}_{1,K} \boldsymbol{v})\|^2_{L^2(K)}. \end{aligned} \tag{14}$$

Note that by scaling, and since $\boldsymbol{\mathcal{P}}_1(K) \subset \boldsymbol{V}(K)$, there holds

$$\begin{aligned} \|\nabla(\boldsymbol{\Pi}_{\boldsymbol{V}} \boldsymbol{v} - \mathbb{P}_{1,K} \boldsymbol{v})\|^2_{L^2(K)} \approx &\sum_{a \in \mathcal{V}_K} |\boldsymbol{\Pi}_{\boldsymbol{V}} \boldsymbol{v}(a) - \mathbb{P}_{1,K} \boldsymbol{v}(a)|^2 \\ &+ \sum_{e \in \mathcal{E}_K} h_e^{-2} \Big| \int_e (\boldsymbol{\Pi}_{\boldsymbol{V}} \boldsymbol{v} - \mathbb{P}_{1,K} \boldsymbol{v})\, ds \Big|^2. \end{aligned} \tag{15}$$

If $a \in \mathcal{V}_K \backslash \mathcal{V}_b$, then we have by (12b),

$$
\begin{aligned}
|\mathbf{\Pi}_{\boldsymbol{V}} \boldsymbol{v}(a) - \mathbb{P}_{1,K}\boldsymbol{v}(a)|^2 =& \Big| \frac{1}{|\mathcal{T}_a|} \sum_{K' \in \mathcal{T}_a} \big(\mathbb{P}_{1,K'}\boldsymbol{v}(a) - \mathbb{P}_{1,K}\boldsymbol{v}(a) \big) \Big|^2 \\
\le& \frac{C}{|\mathcal{T}_a|^2} \sum_{K' \in \mathcal{T}_a} |\mathbb{P}_{1,K'}\boldsymbol{v}(a) - \mathbb{P}_{1,K}\boldsymbol{v}(a)|^2, \qquad (16)
\end{aligned}
$$

where the constant $C > 0$ depends only on the shape regularity of the mesh.

Now for $K, K' \in \mathcal{T}_a$, there exists $\{K_i\}_{i=0}^m \subset \mathcal{T}_a$ such that $K_0 = K$, $K_m = K'$, and K_i and K_{i+1} share a common edge. Thus, by the inverse inequality,

$$
\begin{aligned}
(17)\quad |\mathbb{P}_{1,K'}\boldsymbol{v}(a) - \mathbb{P}_{1,K}\boldsymbol{v}(a)|^2 &\le \sum_{i=0}^{m} |\mathbb{P}_{1,K_{i+1}}\boldsymbol{v}(a) - \mathbb{P}_{1,K_i}\boldsymbol{v}(a)|^2 \\
&\le \sum_{e \in \mathcal{E}_a} \|[\mathbb{P}_1 \boldsymbol{v}]\|_{L^\infty(e)}^2 \le C \sum_{e \in \mathcal{E}_a} h_e^{-1} \|[\boldsymbol{v} - \mathbb{P}_1 \boldsymbol{v}]\|_{L^2(e)}^2.
\end{aligned}
$$

Likewise, if $a \in \mathcal{V}_K \cap \mathcal{V}_b$, then we have by (12c),

$$
(18)\qquad |\mathbf{\Pi}_{\boldsymbol{V}} \boldsymbol{v}(a) - \mathbb{P}_{1,K}\boldsymbol{v}(a)|^2 = |\mathbb{P}_{1,K}\boldsymbol{v}(a)|^2 \le C \sum_{e \in \mathcal{E}_a^b} h_e^{-1} \|[\boldsymbol{v} - \mathbb{P}_1 \boldsymbol{v}]\|_{L^2(e)}^2.
$$

Combining (17)–(18) we obtain

$$
(19)\qquad \sum_{a \in \mathcal{V}_K} |\mathbf{\Pi}_{\boldsymbol{V}} \boldsymbol{v}(a) - \mathbb{P}_{1,K}\boldsymbol{v}(a)|^2 \le C \sum_{a \in \mathcal{V}_K} \sum_{e \in \mathcal{E}_a} h_e^{-1} \|[\boldsymbol{v} - \mathbb{P}_1 \boldsymbol{v}]\|_{L^2(e)}^2.
$$

Now consider the second term in (15). By (12a) and the Cauchy–Schwarz inequality, we have

$$
\begin{aligned}
\sum_{e \in \mathcal{E}_K} h_e^{-2} \Big| \int_e (\mathbf{\Pi}_h \boldsymbol{v} - \mathbb{P}_{1,K}\boldsymbol{v}) ds \Big|^2 &= \sum_{e \in \mathcal{E}_K} h_e^{-2} \Big| \int_e (\boldsymbol{v} - \mathbb{P}_{1,K}\boldsymbol{v}) ds \Big|^2 \\
&\le \sum_{e \in \mathcal{E}_K} h_e^{-1} \|\boldsymbol{v} - \mathbb{P}_{1,K}\boldsymbol{v}\|_{L^2(e)}^2. \qquad (20)
\end{aligned}
$$

Finally we apply (19)–(20) to (15), sum over $K \in \mathcal{T}_h$, use scaling arguments and the shape–regularity of the mesh to get

$$
\begin{aligned}
&\sum_{K \in \mathcal{T}_h} \|\nabla(\mathbf{\Pi}_{\boldsymbol{V}} \boldsymbol{v} - \mathbb{P}_{1,K}\boldsymbol{v})\|_{L^2(K)}^2 \\
\le& C \sum_{K \in \mathcal{T}_h} \Big(\sum_{e \in \mathcal{E}_K} h_e^{-1} \|\boldsymbol{v} - \mathbb{P}_{1,K}\boldsymbol{v}\|_{L^2(e)}^2 + \sum_{a \in \mathcal{V}_K} \sum_{e \in \mathcal{E}_a} h_e^{-1} \|[\boldsymbol{v} - \mathbb{P}_1 \boldsymbol{v}]\|_{L^2(e)}^2 \Big) \\
\le& C \sum_{K \in \mathcal{T}_h} \Big(h_K^{-2} \|\boldsymbol{v} - \mathbb{P}_{1,K}\boldsymbol{v}\|_{L^2(K)}^2 + \|\nabla(\boldsymbol{v} - \mathbb{P}_{1,K})\|_{L^2(K)}^2 \Big)
\end{aligned}
$$

Applying Lemma 2.1 yields $\sum_{K \in \mathcal{T}_h} \|\nabla(\mathbf{\Pi}_{\boldsymbol{V}} \boldsymbol{v} - \mathbb{P}_{1,K}\boldsymbol{v})\|_{L^2(K)}^2 \le C\|\boldsymbol{v}\|_{H^1(\Omega)}$, and so, by using (14), we conclude that $\|\nabla \mathbf{\Pi}_{\boldsymbol{V}} \boldsymbol{v}\|_{L^2(\Omega)} \le C \|\nabla \boldsymbol{v}\|_{L^2(\Omega)}$. □

4.1. Finite Element Method and Convergence Analysis. The finite element method to compute the Stokes problem reads: Find $(\boldsymbol{u}_h, p_h) \in \boldsymbol{V}_h \times W_h$ such that

$$
(21a)\qquad \int_\Omega \nu \nabla \boldsymbol{u}_h : \nabla \boldsymbol{v}\, dx - \int_\Omega (\operatorname{div} \boldsymbol{v}) p_h\, dx = \int_\Omega \boldsymbol{f} \cdot \boldsymbol{v}\, dx, \quad \forall \boldsymbol{v} \in \boldsymbol{V}_h,
$$

$$
(21b)\qquad \int_\Omega (\operatorname{div} \boldsymbol{u}_h) q\, dx = 0, \qquad \forall q \in W_h.
$$

The discrete inf–sup stability given Lemma 4.2 shows that problem (21) is well–posed. In addition we have the following error estimates.

Theorem 4.3. *There holds, for $s = 0, 1, 2,$*

$$\|\boldsymbol{u} - \boldsymbol{u}_h\|_{H^1(\Omega)} \le Ch^s |\boldsymbol{u}|_{H^{s+1}(\Omega)}, \tag{22a}$$

$$\|p - p_h\|_{L^2(\Omega)} \le C\big[h|p|_{H^1(\Omega)} + \nu h^s |\boldsymbol{u}|_{H^{s+1}(\Omega)}\big], \tag{22b}$$

where the constant $C > 0$ is independent of the solution, the discretization parameter, and the viscosity.

Proof. Define the discrete kernel:

$$\boldsymbol{Z}_h = \{\boldsymbol{v} \in \boldsymbol{V}_h : (\operatorname{div} \boldsymbol{v}, q) = 0 \ \forall q \in W_h\} = \{\boldsymbol{v} \in \boldsymbol{V}_h : \operatorname{div} \boldsymbol{v} \equiv 0\}. \tag{23}$$

Restricting (21a) to $\boldsymbol{Z}_h$, reduces the problem to finding $\boldsymbol{u}_h \in \boldsymbol{Z}_h$ such that $\nu(\nabla \boldsymbol{u}_h, \nabla \boldsymbol{v}) = (\boldsymbol{f}, \boldsymbol{v})$ for all $\boldsymbol{v} \in \boldsymbol{Z}_h$. Now since $\boldsymbol{Z}_h$ is divergence–free conforming, we can apply Cea's Lemma and the identity $\boldsymbol{Z}_h = \mathbf{curl}\, \Sigma_h$ to get

$$\|\nabla(\boldsymbol{u} - \boldsymbol{u}_h)\|_{L^2(\Omega)} \le \inf_{\boldsymbol{v} \in \boldsymbol{Z}_h} \|\nabla(\boldsymbol{u} - \boldsymbol{v})\|_{L^2(\Omega)} = \inf_{\varphi \in \Sigma_h} \|\nabla(\boldsymbol{u} - \mathbf{curl}\, \varphi)\|_{L^2(\Omega)}.$$

Writing $\boldsymbol{u}$ in terms of its streamfunction, i.e., $\boldsymbol{u} = \mathbf{curl}\, \psi$ with $\psi \in H^2_0(\Omega)$, we have

$$\|\nabla(\boldsymbol{u} - \boldsymbol{u}_h)\|_{L^2(\Omega)} \le \inf_{\varphi \in \Sigma_h} \|\nabla(\mathbf{curl}(\psi - \varphi))\|_{L^2(\Omega)} = \inf_{\varphi \in \Sigma_h} \|D^2(\psi - \varphi)\|_{L^2(\Omega)}.$$

Employing the approximation properties of Σ_h given in [18, Theorem 6.18] then yields

$$\|\nabla(\boldsymbol{u} - \boldsymbol{u}_h)\|_{L^2(\Omega)} \le Ch^s |\psi|_{H^{s+2}(\Omega)} = Ch^s |\boldsymbol{u}|_{H^{s+1}(\Omega)} \quad s = 0, 1, 2.$$

Finally the inf–sup condition and standard arguments [5] imply that the error of the pressure satisfies

$$\|p_h - \mathbb{P}_W p\|_{L^2(\Omega)} \le \nu \|\nabla(\boldsymbol{u} - \boldsymbol{u}_h)\|_{L^2(\Omega)} \le C\nu h^s |\boldsymbol{u}|_{H^{s+1}(\Omega)}. \tag{24}$$

Applying the triangle inequality and the approximation properties of the L^2 projection then yields (22b). ☐

4.2. A locally post processed pressure solution. Theorem 4.3 shows that the velocity and pressure approximations have different orders of convergence with the pressure solution only converging linearly. In this section, by taking advantage of the superconvergence property (24), we develop a locally computed post–processed pressure solution that has the same quadratic convergence as $\boldsymbol{u} - \boldsymbol{u}_h$.

For an element $K \in \mathcal{T}_h$, let $p_{*,K} \in \mathcal{P}_1(K)$ be the solution to the following discrete Poisson problem with Neumann boundary conditions:

$$\int_K \nabla p_{*,K} \cdot \nabla q \, dx = \int_K \big(\nu \Delta_h \boldsymbol{u}_h + \boldsymbol{f}\big) \cdot \nabla q \, dx \qquad \forall q \in \mathcal{P}_1(K) \tag{25a}$$

$$\int_K p_{*,K} \, dx = \int_K p_h \, dx, \tag{25b}$$

where the discrete Laplacian Δ_h is defined piecewise with respect to K, i.e., $\Delta_h \boldsymbol{u}_h|_{K_i} = \Delta \boldsymbol{u}_h|_{K_i}$ for $i = 1, 2, 3, 4$.

Since $\nabla p_{*,K}$ and ∇q are both constant in (25), we can equivalently write

$$\nabla p_{*,K} \cdot \nabla q = \frac{1}{|K|} \int_K \big(\nu \Delta_h \boldsymbol{u}_h + \boldsymbol{f}\big) \cdot \nabla q \, dx$$

for all $q \in \mathcal{P}_1(K)$. By considering $q = x_i$ we then deduce that the post–processed pressure solution is given by the formula

$$p_{*,K} = C_{*,K} + \frac{\boldsymbol{x}}{|K|} \cdot \int_K \big(\nu \Delta_h \boldsymbol{u}_h + \boldsymbol{f}\big)\, dx \tag{26}$$

with the constant $C_{*,K}$ chosen such that $\int_K p_{*,K}\, dx = \int_K p_h\, dx$.

Theorem 4.4. *Suppose that the solution to the Stokes problem satisfies the regularity $(\boldsymbol{u}, p) \in \boldsymbol{H}^3(\Omega) \times H^2(\Omega)$. Let $p_* \in \mathcal{P}_1(\mathcal{T}_h)$ satisfy* (25) *on each $K \in \mathcal{T}_h$, i.e., $p_*|_K = p_{*,K}$, where $p_{*,K}$ is defined by* (26). *Then there holds*

$$\|p - p_*\|_{L^2(\Omega)} \le Ch^2(\nu |\boldsymbol{u}|_{H^3(\Omega)} + |p|_{H^2(\Omega)}). \tag{27}$$

Proof. As a first step, we claim that $\int_K \big(p - \mathbb{P}_W p\big)\, dx = 0$ for all $K \in \mathcal{T}_h$. To see this, first note that $\int_\Omega (p - \mathbb{P}_W p)\, dx = 0$ since $p, \mathbb{P}_W p \in L^2_0(\Omega)$. Now let $K_1 \in \mathcal{T}_h$ be fixed, and consider $K \in \mathcal{T}_h$ with $K \ne K_1$. Let $q|_{K_1} = 1$, $q|_K = -|K_1|/|K|$, and zero otherwise. Then $q \in W_h \subset L^2_0(\Omega)$, and by the definition of the L^2 projection,

$$\int_{K_1} (p - \mathbb{P}_W p)\, dx = \frac{|K_1|}{|K|} \int_K (p - \mathbb{P}_W p)\, dx.$$

This identity holds for all $K \in \mathcal{T}_h$, and it follows that

$$\begin{aligned} 0 = \int_\Omega (p - \mathbb{P}_W p)\, dx &= \sum_{K \in \mathcal{T}_h} \int_K (p - \mathbb{P}_W p)\, dx \\ &= \sum_{K \in \mathcal{T}_h} \frac{|K|}{|K_1|} \int_{K_1} (p - \mathbb{P}_W p)\, dx = \frac{|\Omega|}{|K_1|} \int_{K_1} (p - \mathbb{P}_W p)\, dx. \end{aligned}$$

We then conclude that $\int_K (p - \mathbb{P}_W p)\, dx = 0$ for all $K \in \mathcal{T}_h$ as claimed.

Next we apply the Poincaré inequality to the difference $p - p_*$ on an element $K \in \mathcal{T}_h$:

$$\|p - p_*\|_{L^2(K)} \le C\big(\|\overline{p - p_*}\|_{L^2(K)} + h_K \|\nabla(p - p_*)\|_{L^2(K)}\big), \tag{28}$$

where $\overline{p - p_*}$ denotes the mean of $(p - p_*)$ over K. Since

$$\overline{p - p_*} = \overline{p} - \overline{p_*} = \overline{\mathbb{P}_W p} - \overline{p_h} = \overline{\mathbb{P}_W p - p_h},$$

we obtain

$$\|\overline{p - p_*}\|_{L^2(K)} = \|\overline{\mathbb{P}_W p - p_h}\|_{L^2(K)} \le \|\mathbb{P}_W p - p_h\|_{L^2(K)}. \tag{29}$$

On the other hand, by (25) and the Cauchy–Schwarz inequality, we have for all $q \in \mathcal{P}_1(K)$,

$$\begin{aligned} &\|\nabla(p - p_*)\|^2_{L^2(K)} \\ &= \int_K \nabla(p - p_*) \cdot \nabla(p - q)\, dx + \int_K \nabla(p - p_*) \cdot \nabla(q - p_*)\, dx \\ &= \int_K \nabla(p - p_*) \cdot \nabla(p - q)\, dx + \int_K \nu(\Delta_h(\boldsymbol{u} - \boldsymbol{u}_h) \cdot \nabla(q - p_*)\, dx \\ &\le \|\nabla(p - p_*)\|_{L^2(K)} \|\nabla(p - q)\|_{L^2(K)} + \nu \|\Delta_h(\boldsymbol{u} - \boldsymbol{u}_h)\|_{L^2(K)} \|\nabla(q - p_*)\|_{L^2(K)}. \end{aligned}$$

An application of the triangle inequality then yields

$$\|\nabla(p - p_*)\|_{L^2(K)} \le C\big(\|\nabla(p - q)\|_{L^2(K)} + \nu \|\Delta_h(\boldsymbol{u} - \boldsymbol{u}_h)\|_{L^2(K)}\big) \quad \forall q \in \mathcal{P}_1(K). \tag{30}$$

Applying the estimates (29)–(30) to (28), summing over $K \in \mathcal{T}_h$, and then applying (24) and standard interpolation estimates yield

$$\begin{aligned}\|p-p_*\|^2_{L^2(\Omega)} &\le C(\|p_h - P_h p\|^2_{L^2(\Omega)} \\ &\quad + \inf_{q\in\mathcal{P}_1(\mathcal{T}_h)} \sum_{K\in\mathcal{T}_h} h_K^2\big(\nu^2\|\Delta_h(\boldsymbol{u}-\boldsymbol{u}_h)\|^2_{L^2(K)} + \|\nabla(p-q)\|^2_{L^2(K)}\big) \\ &\le C\Big(h^4\big(\nu^2|\boldsymbol{u}|^2_{H^3(\Omega)} + |p|^2_{H^2(\Omega)}\big) + \sum_{K\in\mathcal{T}_h} h_K^2\nu^2\|\Delta_h(\boldsymbol{u}-\boldsymbol{u}_h)\|^2_{L^2(K)}\Big).\end{aligned} \tag{31}$$

By the triangle and inverse inequalities, we have for any $\boldsymbol{v}\in\boldsymbol{\mathcal{P}}_2(K_r)\cap\boldsymbol{H}^1(K)$,

$$\begin{aligned}&h_K\|\Delta_h(\boldsymbol{u}-\boldsymbol{u}_h)\|_{L^2(K)} \\ \le& h_K\|\Delta_h(\boldsymbol{u}-\boldsymbol{v})\|_{L^2(K)} + C\|\nabla(\boldsymbol{u}_h-\boldsymbol{v})\|_{L^2(K)} \\ \le& h_K\|\Delta_h(\boldsymbol{u}-\boldsymbol{v})\|_{L^2(K)} + C\big(\|\nabla(\boldsymbol{u}-\boldsymbol{v})\|_{L^2(K)} + \|\nabla(\boldsymbol{u}-\boldsymbol{u}_h)\|_{L^2(K)}\big).\end{aligned}$$

By taking $\boldsymbol{v}$ to be the nodal interpolant of $\boldsymbol{u}$ we have

$$h_K\|\Delta_h(\boldsymbol{u}-\boldsymbol{u}_h)\|_{L^2(K)} \le C\big(h_K^2|\boldsymbol{u}|_{H^3(K)} + \|\nabla(\boldsymbol{u}-\boldsymbol{u}_h)\|_{L^2(K)}\big).$$

Applying this estimate to (31) and applying estimate (22a) then gets

$$\begin{aligned}\|p-p_*\|^2_{L^2(\Omega)} &\le C\Big(h^4\big(\nu^2|\boldsymbol{u}|^2_{H^3(\Omega)} + |p|^2_{H^2(\Omega)}\big) + \nu^2\|\nabla(\boldsymbol{u}-\boldsymbol{u}_h)\|^2_{L^2(\Omega)}\Big) \\ &\le Ch^4\big(\nu^2|\boldsymbol{u}|^2_{H^3(\Omega)} + |p|^2_{H^2(\Omega)}\big).\end{aligned}$$

Taking the square root of this last expression yields (27). □

5. Implementation Aspects

In this section we describe the construction of the velocity space $\boldsymbol{V}_h$, and in particular, how to compute and implement a basis of this space. We note that, unlike the Taylor–Hood pair, the local velocity space is defined on a physical element of the mesh, and it is *not* invariant under bilinear mappings. These restrictions may suggest that the basis must be solved locally on each quadrilateral of the mesh (thus leading to sixteen 16×16 linear systems for each element). Below we discuss an alternative construction, which, besides being more efficient, may possibly be extended to isoparametric elements.

Let K be a quadrilateral in the mesh, and let $\{T_1, T_2\}$ be two triangles obtained by splitting K from opposite vertices. Let $A=(A_1,A_2)$ be the unique vertex of T_2 that is not a vertex of T_1. Let $\hat{T}$ be the reference simplex with vertices $(0,0),(1,0),(0,1)$, and let $F:\hat{T}\to T_1$ be an affine bijection onto T_1. We then set $\hat{T}_2 := F^{-1}(T_2)$ and $\hat{A}=(\hat{A}_1,\hat{A}_2) := F^{-1}(A)$, and define $\hat{K}_{\hat{A}} := \hat{T}_1\cup\hat{T}_2$, which is a convex quadrilateral with vertices $(1,0),(\hat{A}_1,\hat{A}_2),(0,1),(0,0)$; cf. Figure 5. By construction, $F:\hat{K}_{\hat{A}}\to K$ is an affine bijection.

Write $F(\hat{x}) = B\hat{x}+b$ with $B\in\mathbb{R}^{2\times2}$ and $b\in\mathbb{R}^2$. Let $\{\hat{a}_j\}_{j=1}^8$ be the set of (exterior) vertices and edge midpoints of $\hat{K}_{\hat{A}}$, and let $\{\hat{\boldsymbol{v}}_i^{(k)}\}\subset\boldsymbol{V}(\hat{K})$ satisfy $\hat{\boldsymbol{v}}_i^{(k)}(\hat{a}_j) = \boldsymbol{e}_k\delta_{i,j}$ for $i,j=1,2,\ldots,8$ and $k=1,2$; that is, $\{\hat{\boldsymbol{v}}_i^{(k)}\}$ is the canonical basis of $\boldsymbol{V}(\hat{K}_{\hat{A}})$ induced by Lemma 3.5. We then define $\boldsymbol{v}_i^{(k)}$ via a modified Piola transform:

$$\boldsymbol{v}_i^{(k)}(x) = B\big(\beta_1^{(k)}\hat{\boldsymbol{v}}_i^{(1)}(\hat{x}) + \beta_2^{(k)}\hat{\boldsymbol{v}}_i^{(2)}(\hat{x})\big) \qquad \text{for } \hat{x}\in\hat{K}_{\hat{A}}, \tag{32}$$

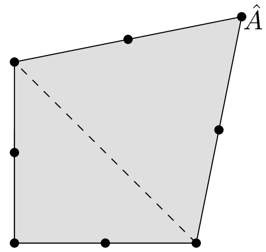

FIGURE 2. Skewed reference element $\hat{K}_{\hat{A}}$ with vertices $(1,0), (\hat{A}_1, \hat{A}_2), (0,1), (0,0)$.

with

$$\begin{pmatrix} \beta_1^{(k)} \\ \beta_2^{(k)} \end{pmatrix} := B^{-1}\boldsymbol{e}_k,$$

and $x = F(\hat{x})$. Clearly $\boldsymbol{v}_i^{(k)} \in \boldsymbol{\mathcal{P}}_2(K_r) \cap \boldsymbol{H}^1(K)$. Moreover, computing the divergence of $\boldsymbol{v}_i^{(k)}$ we find

$$\operatorname{div} \boldsymbol{v}_i^{(k)}(x) = \beta_1^{(k)} \widehat{\operatorname{div}}\, \hat{\boldsymbol{v}}_i^{(1)}(\hat{x}) + \beta_2^{(k)} \widehat{\operatorname{div}}\, \hat{\boldsymbol{v}}_i^{(2)}(\hat{x}) = \beta_1^{(k)} \widehat{\operatorname{div}}\, \hat{\boldsymbol{v}}_i^{(1)} + \beta_2^{(k)} \widehat{\operatorname{div}}\, \hat{\boldsymbol{v}}_i^{(2)},$$

where the last equality emphasizes that the divergence of $\hat{\boldsymbol{v}}_i^{(k)}$ is constant on $\hat{K}$. Thus, $\boldsymbol{v}_i^{(k)} \in \boldsymbol{V}(K)$. We also find that on the (physical) nodes $a_j = F(\hat{a}_j)$,

$$\begin{aligned} \boldsymbol{v}_i^{(k)}(a_j) &= B\big(\beta_1^{(k)} \hat{\boldsymbol{v}}_i^{(1)}(\hat{a}_j) + \beta_2^{(k)} \hat{\boldsymbol{v}}_i^{(2)}(\hat{a}_j)\big) \\ &= B\big(\beta_1^{(k)} \delta_{i,j} \boldsymbol{e}_1 + \beta_2^{(k)} \delta_{i,j} \boldsymbol{e}_2\big) \\ &= \delta_{i,j} B \begin{pmatrix} \beta_1^{(k)} \\ \beta_2^{(k)} \end{pmatrix} = \delta_{i,j} \boldsymbol{e}_k. \end{aligned}$$

Thus, $\{\boldsymbol{v}_i^{(k)}\}$ is the canonical basis of $\boldsymbol{V}(K)$.

To summarize, to compute the local velocity basis on an element $K \in \mathcal{T}_h$, we first take three vertices of K to construct an (inverse) affine mapping and a skewed reference element which is parameterized by the vertex $\hat{A}$. A basis on the skewed reference element is computed, and the physical bases are found via the transformation (32). To finalize our discussion, we describe an efficient way to compute the basis on the skewed reference element $\hat{K}_{\hat{A}}$.

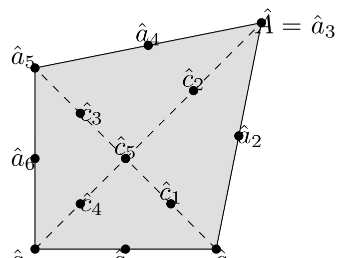

FIGURE 3. Labelling of skewed reference quadrilateral

Let $\{\hat{c}_j\}_{j=1}^4$ denote the set of interior edge midpoints of a two–diagonal split of $\hat{K}_{\hat{A}}$, and let $\hat{c}_5$ be the point of intersection of the two diagonals; cf. Figure 3. Let

$\{\hat{w}_i\}_{i=1}^5 \subset \mathcal{P}_2(\hat{K}_{\hat{A},r}) \cap H^1(\hat{K}_{\hat{A}})$ and $\{\hat{v}_i\}_{i=1}^8 \subset \mathcal{P}_2(\hat{K}_{\hat{A},r}) \cap H^1(\hat{K}_{\hat{A}})$ satisfy

$$\hat{w}_i(c_j) = \delta_{i,j}, \qquad \hat{w}_i(a_j) = 0,$$
$$\hat{v}_i(c_j) = 0, \qquad \hat{v}_i(a_j) = \delta_{i,j}.$$

Thus, $\{\hat{w}_i, \hat{v}_i\}$ form the canonical basis of $\mathcal{P}_2(\hat{K}_{\hat{A},r}) \cap H^1(\hat{K}_{\hat{A}})$ (the Lagrange basis). Note that $\hat{w}_i$ vanishes on $\partial\hat{K}_{\hat{A}}$, and that $\{\hat{w}_i\boldsymbol{e}_k, \hat{v}_i\boldsymbol{e}_k\}$ forms the canonical basis of $\boldsymbol{\mathcal{P}}_2(\hat{K}_{\hat{A},r}) \cap \boldsymbol{H}^1(\hat{K}_{\hat{A}})$.

We view the basis of $\boldsymbol{V}(\hat{K}_{\hat{A}})$ as the the Lagrange sub–basis $\{\hat{v}_i\boldsymbol{e}_k\}$ "corrected" by the functions $\hat{w}_i$ to enforce the constant divergence constraint. In particular, Lemma 3.5 implies the following result.

Lemma 5.1. *Let $\{\boldsymbol{v}_i^{(k)}\}$ denote the canonical basis of $\boldsymbol{V}(\hat{K}_{\hat{A}})$. Then, for each i and k, there exist unique vectors $\{\boldsymbol{\alpha}_{i,j}^{(k)}\}_{j=1}^5 \subset \mathbb{R}^2$ such that*

$$\hat{\boldsymbol{v}}_i^{(k)} = \boldsymbol{e}_k\hat{v}_i + \sum_{j=1}^5 \boldsymbol{\alpha}_{i,j}^{(k)}\hat{w}_j.$$

In particular, the vectors are uniquely determined the following constraint, which represents a 10×10 system:

$$\widehat{\operatorname{div}}\,\hat{\boldsymbol{v}}_i^{(k)} = \boldsymbol{e}_k \cdot \hat{\nabla}\hat{v}_i + \sum_{j=1}^5 \boldsymbol{\alpha}_{i,j}^{(k)} \cdot \hat{\nabla}\hat{w}_j \in \mathcal{P}_0(\hat{K}_{\hat{A}}). \tag{33}$$

Remark 5.2. *The 10×10 system (33) can be easily solved symbolically in terms of the point $\hat{A}$ and hardcoded into a finite element subroutine.*

6. Numerical Examples

In this section, we perform some numerical experiments which back up the theoretical results in Section 4. In addition, we compare the performance of the proposed method with the reduced (serendipity) Taylor–Hood finite element pair with grad-div stabilization.

6.1. Convergence Rate Tests. In these series of tests, the domain is the unit square $\Omega = (0, 1)$, the viscosity is $\nu = 10^{-2}$, and the data is chosen such that the exact solution is given by

$$\begin{aligned} &\boldsymbol{u} = \mathbf{curl}\,\psi, \qquad \psi = \sin^2(3\pi x_1)\sin^2(3\pi x_2),\\ &p = x_1 - x_2. \end{aligned} \tag{34}$$

We compute the finite element method (21) on a sequence of refined meshes, obtained from a $\mathcal{O}(h)$ perturbation of a uniform grid (see Figure 6.1), and report the errors and rates of convergence in Table 1. The table clearly shows third and second order convergence of the velocity approximation measured in the L^2 and H^1 norms, respectively. In addition, the pressure approximation is first order convergent, and the post-processed pressure solution is second order convergent. These rates of convergence agree with the theoretical results established in Theorems 4.3–4.4.

For comparison, the errors using the reduced Taylor–Hood element pair $\tilde{Q}_2 - Q_1$ with grad-div stabilization on the same sequence of meshes are listed in Table 2. The grad-div stabilization parameter is taken to be one in the tests.

Tables 1–2 show that the errors of the divergence–free yielding method are considerable smaller than the Taylor–Hood method. In addition, we observe a deterioration of the convergence rate of the Taylor–Hood method as the mesh is refined.

This behavior is expected since the quadrilaterals in the mesh are not affine equivalent [2].

TABLE 1. Errors and rates of convergence of the divergence-free yielding method on a sequence of mesh refinements. The exact solution is given by (34).

h	$\|\boldsymbol{u}-\boldsymbol{u}_h\|_{L^2}$	rate	$\|\nabla(\boldsymbol{u}-\boldsymbol{u})\|_{L^2}$	rate	$\|p-p_h\|_{L^2}$	rate	$\|p-p_*\|_{L^2}$	rate	V^*
2^{-2}	3.07E+00		8.85E+01		1.56E-01		7.16E-01		1.99E-13
2^{-3}	5.44E-01	2.50	3.06E+01	1.53	6.02E-02	1.38	2.88E-01	1.32	5.49E-13
2^{-4}	6.96E-02	2.97	7.94E+00	1.95	2.72E-02	1.14	5.32E-02	2.43	3.24E-12
2^{-5}	9.24E-03	2.91	2.10E+00	1.92	1.34E-02	1.02	1.09E-02	2.29	3.82E-12
2^{-6}	1.17E-03	2.98	5.35E-01	1.98	6.70E-03	1.00	2.53E-03	2.11	2.37E-11
2^{-7}	1.43E-04	3.03	1.32E-01	2.02	3.34E-03	1.01	5.98E-04	2.08	1.03E-10
2^{-8}	1.78E-05	3.01	3.30E-02	2.00	1.67E-03	1.00	1.48E-04	2.02	2.20E-10
2^{-9}	2.22E-06	3.00	8.24E-03	2.00	8.35E-04	1.00	3.69E-05	2.00	7.04E-10

V^* stands for $\|\operatorname{div} \boldsymbol{u}_h\|_{L^\infty}$

TABLE 2. Errors and rates of convergence of the reduced Taylor–Hood method with grad–div stabilization on a sequence of mesh refinements. The exact solution is given by (34).

h	$\|\boldsymbol{u}-\boldsymbol{u}_h\|_{L^2}$	rate	$\|\nabla(\boldsymbol{u}-\boldsymbol{u})\|_{L^2}$	rate	$\|p-p_h\|_{L^2}$	rate	$\|\operatorname{div} \boldsymbol{u}_h\|_{L^\infty}$
2^{-2}	5.89E+00		1.17E+02		2.08E+00		6.67E+00
2^{-3}	1.68E+00	1.81	4.63E+01	1.34	1.03E+00	1.02	4.39E+00
2^{-4}	1.56E-01	3.43	8.16E+00	2.50	1.36E-01	2.92	2.27E+00
2^{-5}	1.91E-02	3.03	1.96E+00	2.06	5.40E-02	1.33	1.10E+00
2^{-6}	2.62E-03	2.87	6.55E-01	1.58	4.76E-03	3.51	2.47E-01
2^{-7}	3.95E-04	2.73	2.57E-01	1.35	1.16E-03	2.03	1.27E-01
2^{-8}	7.80E-05	2.34	1.22E-01	1.08	5.06E-04	1.20	7.90E-02
2^{-9}	1.79E-05	2.12	6.00E-02	1.02	2.37E-04	1.09	4.54E-02

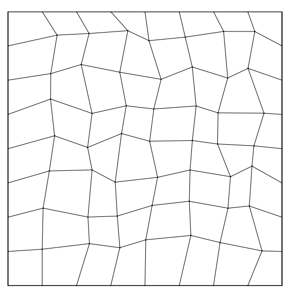

FIGURE 4. The quadrilateral mesh used in Section 6.1 with $h = 2^{-3}$.

6.2. Non-isothermal Flow Example. In this section, we use the proposed spaces to compute a natural convection problem modeled by the Navier–Stokes–Boussinesq system:

$$\begin{aligned} -\nu\Delta\boldsymbol{u} + (\boldsymbol{u}\cdot\nabla)\boldsymbol{u} + \nabla p &= \mathrm{Ra}\boldsymbol{e}_2\varphi, \\ \operatorname{div}\boldsymbol{u} &= 0, \\ -\Delta\varphi + \boldsymbol{u}\cdot\nabla\varphi &= 0. \end{aligned} \tag{35}$$

Here, φ represents the temperature, and Ra is the (rescaled) Rayleigh number, representing the relative strength of buoyancy forces with respect to thermal and momentum diffusion [16, 9].

The domain is taken to be $\Omega = (0,1)^2 \backslash (S_1 \cup S_2)$, where S_1 is the triangle with vertices $(1,1)$, $(0.5, 0.5)$, $(1, 0.5)$, and S_2 is the regular polygon centered at $(15/32, 41/50)$ and with edge length $1/16$. The system of equations is coupled with velocity no–slip boundary conditions, heating/cooling is applied on the top and middle horizontal sides

$$\varphi = 10 \qquad \text{on } \Gamma_1 := (0,1) \times \{1\},$$
$$\varphi = 0 \qquad \text{on } \Gamma_2 := (1/2, 1) \times \{1/2\},$$

and the rest of the boundary is insulated:

$$\frac{\partial \varphi}{\partial \boldsymbol{n}} = 0 \qquad \text{on } \partial\Omega \backslash (\Gamma_1 \cup \Gamma_2).$$

We note that large Rayleigh numbers induce a large rotation–free part of the forcing function in the momentum equations, which has a significant effect on the discrete solutions if the divergence–free constraint is not sufficiently resolved [16].

Figure 6.2 shows the resulting computing streamlines and temperature profiles with $\text{Ra} = 2 \times 10^4$ and $\nu = 3.5 \times 10^{-2}$ on relative course meshes using the grad–div stabilized Taylor–Hood finite element pair with 8709 unknowns (left) and the divergence–free yielding method with 8657 unknowns (middle). In both cases, the temperature is approximated by the biquadratic Lagrange finite element space. The numerical experiments clearly show the advantage of the divergence-free yielding pair, as the method resolves the prominent features of the flow on a relatively course grid.

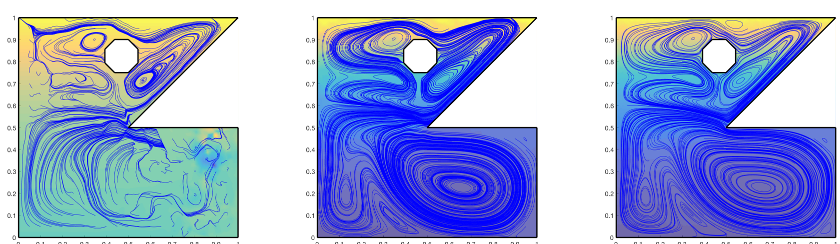

FIGURE 5. Streamlines and pressure profiles of the Boussinesq system (35) with $\nu = 3.5 \times 10^{-2}$ and $\text{Ra} = 2 \times 10^4$. Left: Taylor–Hood with grad-div stabilization (8709 unknowns); Middle: Divergence-free yielding method (8657 unknowns); Right: Reference solution (412k unknowns).

7. Conclusions

In this paper we introduced a stable finite element pair for the Stokes problem that enforces the divergence–free condition exactly in the method. The key features of the method are its relative low–order and robustness with respect to the meshes. In the future we plan on extending these results to the three–dimensional setting.

8. Acknowledgments

This research was partially supported by NSF grants DMS-1417980 and DMS-1719829, and the Alfred Sloan Foundation.

References

[1] P. Alfeld and T. Sorokina, Linear differential operators on bivariate spline spaces and spline vector fields, BIT, 56(1):15–32, 2016.

[2] D.N. Arnold, D. Boffi, and R.S. Falk, Approximation by quadrilateral finite elements, Math. Comp., 71(239):909–922, 2002.

[3] T.M. Austin, T.A. Manteuffel, S. McCormick, A robust multilevel approach for minimizing $H(div)$-dominated functionals in an H^1-conforming finite element space, Numer. Linear Algebra Appl., 11(2-3):115–140, 2004.

[4] M.A. Belenli, L.G. Rebholz, and F. Tone, A note on the importance of mass conservation in long-time stability of Navier-Stokes simulations using finite elements, Appl. Math. Lett., 45:98–102, 2015.

[5] D. Boffi, F. Brezzi, L. Demkowicz, R. Durán, R.S. Falk, and M. Fortin, Mixed finite elements, compatibility conditions, and applications., Lectures given at the C.I.M.E. Summer School held in Cetraro, June 26–July 1, 2006. Edited by Boffi and Lucia Gastaldi. Lecture Notes in Mathematics, 1939. Springer-Verlag, Berlin; Fondazione C.I.M.E., Florence, 2008.

[6] A. Buffa, C. de Falco, and G. Sangalli, IsoGeometric Analysis: stable elements for the 2D Stokes equation, Internat. J. Numer. Methods Fluids, 65(11-12):1407–1422, 2011.

[7] S.H. Christiansen and H. Kaibo, Generalized Finite Element Systems for smooth differential forms and Stokes problem, arXiv:1605.08657 [math.NA].

[8] P.G. Ciarlet, The finite element method for elliptic problems, Reprint of the 1978 original, Classics in Applied Mathematics, 40, SIAM, Philadelphia, PA, 2002.

[9] A. Cibik and S. Kaya, A projection-based stabilized finite element method for steady-state natural convection problem, J. Math. Anal. Appl., 381(2):469–484, 2011.

[10] J.F. Ciavaldini and J.-C. Nedelec, Sur l'element de Fraeijs de Verbeke et Sander, Rev. Francaise Automat. Informat. Recherche Operationnelle Ser. Rouge, 8(R-2):29–46, 1974.

[11] F. de Verbeke A conforming finite element for plate bending, J. Solids Structure, 108:4–95, 1968.

[12] J. Douglas, T. Dupont, P. Percell, and R. Scott, A family of C^1 finite elements with optimal approximation properties for various Galerkin methods for 2nd and 4th order problems, RAIRO Anal. Numer., 13(3):227–255, 1979.

[13] A. Ern and J.-L. Guermond, Theory and practice of finite elements, Applied Mathematical Sciences, 159, Springer-Verlag, New York, 2004.

[14] J.A. Evans and T.J.R. Hughes, Isogeometric divergence-conforming B-splines for the steady Navier-Stokes equations, Math. Models Methods Appl. Sci., 23(8):1421–1478, 2013.

[15] R.S. Falk and M. Neilan, Stokes complexes and the construction of stable finite elements with pointwise mass conversation, SIAM J. Numer. Anal., 51(2):1308–1326, 2013.

[16] K.J. Galvin, A. Linke, L.G. Rebholz, and N.E. Wilson, Stabilizing poor mass conservation in incompressible flow problems with large irrotational forcing and application to thermal convection, Comput. Methods Appl. Mech. Engrg., 237/240:166–176, 2012.

[17] J. Guzmán and M. Neilan, Conforming and divergence-free Stokes elements on general triangular meshes, Math. Comp., 83(285):14–36, 2014.

[18] M.-J. Lai and L.L. Schumaker, Spline functions on triangulations, Encyclopedia of Mathematics and its Applications, 110. Cambridge University Press, Cambridge, 2007.

[19] J. Morgan and L.R. Scott, A nodal basis for C^1 piecewise polynomials of degree $n \geq 5$, Math. Comput., 29:736–740, 1975.

[20] M. Neilan and D. Sap, Stokes elements on cubic meshes yielding divergence-free approximations, Calcolo, 53(3):263–283, 2016.

[21] G. Sander, Bornes superieures et inferieures dans l'analyse matricielle des plaques flexion-torsion, Bull. Soc. Roy. Sci. Liege, 494:33–456,1964.

[22] L.R. Scott and M. Vogelius, Norm estimates for a maximal right inverse of the divergence operator in spaces of piecewise polynomials, RAIRO Modél. Math. Anal. Numér, 19(1):111–143, 1985.

[23] R. Stenberg, Analysis of mixed finite element methods for the Stokes problem: a unified approach, Math. Comp., 42(165):9–23, 1984.

[24] M. Vogelius, A right-inverse for the divergence operator in spaces of piecewise polynomials. Application to the p-version of the finite element method, Numer. Math., 41(1):19–37, 1983.

[25] S. Zhang, A family of $Q_{k+1,k} \times Q_{k,k+1}$ divergence-free finite elements on rectangular grids, SIAM J. Numer. Anal., 47(3):2090–2107, 2009.

[26] S. Zhang, Stable finite element pair for Stokes problem and discrete Stokes complex on quadrilateral grids, Numer. Math., 133(2):371–408, 2016.

Department of Mathematics, University of Pittsburgh, Pittsburgh, PA 15226 USA
E-mail: neilan@pitt.edu and dus8@pitt.edu
URL: http://www.pitt.edu/~neilan/